TDA Progress Report 42-100

February 15, 1990

12 P.

Dual-Shaped Offset Reflector Antenna Designs From Solutions of the Geometrical Optics First-Order Partial Differential Equations

V. Galindo-Israel and W. Imbriale
Ground Antenna and Facilities Engineering Section

K. Shogen and R. Mittra
Electromagnetic Communications Laboratory
University of Illinois, Urbana, IL

In obtaining solutions to the first-order nonlinear partial differential equations (PDEs) for synthesizing offset dual-shaped reflectors, it is found that previously observed computational problems can be avoided if the integration of the PDEs is started from an inner projected perimeter and integrated outward rather than starting from an outer projected perimeter and integrating inward. This procedure, however, introduces a new parameter, the main reflector inner perimeter radius ρ_0, when given a subreflector inner angle θ_0. Furthermore, a desired outer projected perimeter (e.g., a circle) is no longer guaranteed. "Stability" of the integration is maintained if some of the initial parameters are determined first from an approximate solution to the PDEs. A one-, two-, or three-parameter optimization algorithm can then be used to obtain a "best" set of parameters yielding a close fit to the desired projected outer rim. Good low cross-polarization mapping functions are also obtained. These methods are illustrated by synthesis of a high-gain offset-shaped Cassegrainian antenna and a low-noise offset-shaped Gregorian antenna.

I. Introduction

The problem of synthesizing dual-shaped offset reflector antennas has received considerable attention in recent years, not only because it is theoretically challenging but also because it is of considerable practical interest. Galindo-Israel et al. [1] presented an exact algorithm for simultaneously synthesizing the shapes of the sub and main reflectors for an arbitrary feed pattern, aperture amplitude, and phase distributions by solving a set of nonlinear first-order partial differential equations (PDEs). Jervase et al. [2] discussed an extension of the numerical method presented in [1] and gave some computed results for the reflector shapes. It has been observed that numerical difficulties may arise when applying these techniques, especially in the vicinity of the center region of the reflectors. This occurs when the PDEs' integration is initialized on the outer rims of the reflectors and proceeds "inward" [1].

In this article, we investigate the possibility of circumventing these difficulties by starting the synthesis procedure not from the periphery, but from inner or central rims of the reflectors with the integration then proceeding "outward" to the outer rims. The success of this procedure depends significantly on the initial conditions chosen at the inner rims. An approximate solution to the synthesis problem provides one good choice for the initial conditions. Numerical results for symmetric feed patterns and aperture distributions are included to illustrate the application of the synthesis procedure based on a "center" start. A uniform aperture distribution for a high-gain dual-offset shaped Cassegrainian-type reflector antenna is illustrated first. Next, an aperture distribution that is uniform over most of the aperture, but is given a Gaussian taper near the outer rim, is shown in a Gregorian-type configuration. This distribution is useful for a low-noise (but high-gain) large ground antenna where very low spillover is desired past the main reflector into a "hot" ground background.

Starting the integration in the central region of the reflectors and integrating outward does *not* guarantee a circular projected outer rim as integrating inward does (if that is desirable). It is possible to *optimize* one or more initial parameters to obtain a desired circular outer rim (or other desired results). This approach was investigated for obtaining a circular projected outer rim with very good results.

II. Numerical Method

We choose the specified feed power pattern $I(\theta)$ and the desired aperture power distribution $V(\rho)$ to be circularly symmetric. For the antenna system shown in Fig. 1, the differential equations for synthesizing the dual reflector system are given by [1]:

$$r_\theta = r_\theta(\theta, \phi|\rho, \psi, r) \tag{1}$$

$$r_\phi = r_\phi(\theta, \phi|\rho, \psi, r) \tag{2}$$

$$\rho_\theta = \rho_\theta(\theta, \phi|\rho, \psi, r; \rho_\phi, \psi_\phi) \tag{3}$$

$$\psi_\theta = \psi_\theta(\theta, \phi|\rho, \psi, r; \rho_\phi, \psi_\phi) \tag{4}$$

Equations (1) and (2) are obtained by applying Snell's Law to the subreflector while z is calculated by using the path length condition viz., $r + S - z =$ constant. Equations (3) and (4) are obtained from the following three conditions:

(A) Conservation of energy on a pointwise basis for geometrical optics:

$$V_c V(\rho)\rho[\rho_\theta \psi_\phi - \rho_\phi \psi_\theta] = I(\theta)\sin\theta \tag{5}$$

$$V_c = \int_0^{\theta_M} I(\theta)\sin\theta d\theta \Big/ \int_0^{\rho_M} V(\rho)\rho d\rho \tag{6}$$

(B) Total differentiability at all points $(\theta, \phi, \rho, \psi)$

$$r_{\theta\phi} = r_{\phi\theta} \tag{7}$$

(C) Snell's Law applied to the main reflector.

Equations (1) through (4) are solved by starting with some initial values for ρ, θ (very small), and ψ, and then increasing θ in small increments to obtain the main and the subreflector surfaces in a progressive manner. The procedure is identical to that in [1] except that the integration is outward (increasing θ and ρ).

III. Numerical Results for the Cassegrainian-Type System

Results are presented for the following system parameters: $a = 11$, $\Omega = 21°$, $\theta_M = 16°$, $\rho_M = 5$, $r_i = 7$ (see Fig. 1). The optical path length is assumed to be 22, the specified or object aperture power distribution is uniform, and the feed pattern is taken to be $\cos^n\theta$ with $n = 151$ (yielding a subreflector edge illumination level at -25.9 dB below the center illumination).

As mentioned above, the reflector shapes depend strongly on the initial values chosen for the solution of the differential Eqs. (1) through (4). For a given θ_0 (minimum θ rim value for the subreflector), a critical initial parameter is the value chosen for ρ_0 (minimum ρ rim value for the main reflector). As an example, Fig. 2 shows two results for the same system parameters but with different initial values of ρ_0. It is observed from this figure that ρ_θ becomes very large near the center point ($\theta \approx 0$) for one of the ρ_0 choices (case B). This leads to unacceptable reflector shapes.

One approach to finding good initial values is to start with an approximate solution (see [3], for example). An approximate solution can be found by relaxing the total differentiability condition (i.e., Eq. 7), and then prescribing the mapping [1,3] in advance as $\psi = \phi$, $\psi_\phi = 1$, $\rho_\phi = 0$, and $\psi_\theta = 0$. Under these conditions the mapping from (θ, ϕ) to (ρ, ψ) is forced to be concentric. Thus the conservation of energy reduces to

$$V_c V(\rho)\rho\rho_\theta = I(\theta)\sin\theta \tag{8}$$

The above *approximate* solution [3] allows a value of ρ_0 to be found for a given θ_0 which then yields very good and stable numerical solutions by the exact method discussed earlier. While this value of ρ_0 is not *critical* for obtaining a "good" solution, it is critical if a perfectly circular (or other shape) is required for the *outer* rim of the main reflector. Alternate methods for choosing ρ_0 will be discussed in the next section.

Figure 3 presents the results for ψ_θ versus θ for two cases in order to illustrate the advantage of starting from a central rim instead of the outer edge. Note that the outward solution (solid line) exhibits a much better behavior than the corresponding inward solution (dashed line). Figure 4 shows the main and subreflector shapes derived by using the outward approach. Note that not only are the surfaces well-behaved, but also that the maximum value of ρ of the main reflector in this case does not deviate significantly from ρ_M, the value for maximum ρ, which was desired to be 5. Thus, the outer periphery condition, that the projected aperture be circular, is approximated very well in this solution.

Figure 5 shows a comparison between the radiation patterns in the offset plane of the shaped reflector (solid line) and a comparable Cassegrainian antenna. The diameter of the main reflectors of the two antennas is 80λ. The system parameters of the shaped reflector are $A = 2200$, $\Omega = 23°$, $\theta_M = 8.5°$, $\rho_M = 1000$, $r_i = 1000$ (see Fig. 1). The optical units of length can be converted to wavelengths by dividing by 25. The optical path length is assumed to be 4000. The specified main reflector aperture amplitude distribution was uniform and the feed pattern was taken to be $\cos^n \theta$, with $n = 151$. The radiation patterns are calculated by using geometrical optics for the subreflector and physical optics for the main reflector scattering. Some radiation characteristics of the two antennas are given in Table 1.

IV. Obtaining a Gregorian Design by Optimization of Parameters

In this section, we will discuss a special offset dual-shaped Gregorian design wherein the parameter ρ_0 and other initial parameters as well are set by an optimization procedure.

The synthesis software used herein can go through a complete integration in less than a half minute on a 386 20-MHz processor when approximately eight Fourier terms are used to represent *differences* in the functions

$$\rho(\phi) \text{ and } \psi(\phi) \tag{9}$$

between adjacent θ values. Since an FFT is used for representation of these functions, the increase in time with increasing number of Fourier terms is linear. Eight Fourier terms was sufficient for the case to be presented.

This very rapid two-dimensional integration of the nonlinear PDEs reasonably allows for the possibility of performing the integration *many times* in an optimization algorithm to "optimize" one or more initial parameters.

One parameter that can be optimized is the choice of ρ_0 for a given θ_0 value. Ideally, a value of ρ_0 can be chosen at the start of the optimization by solving for the approximate solution to the PDEs as discussed earlier.

The question immediately arises as to what object function the optimization algorithm should attempt to minimize. One useful object is a perfectly circular projected perimeter of the main reflector at $\theta = \theta_{MAX}$. Thus, the function

$$f = SQRT\left[\sum_{n=1}^{N}(\rho_{M_i} - \rho_M)^2/N\right] \tag{10}$$

can be minimized, where

$$(\rho_{M_i} : i = 1, ..., N) \tag{10a}$$

are the perimeter values obtained at the set

$$(\phi_i : i = 1, ..., N) \text{ or } (\psi_i : i = 1, ..., N) \tag{10b}$$

for any given integration of initial parameter values. The value ρ_M need not be a constant unless a circular perimeter is desired. The object function could be expanded to obtain a prescribed set of mapping functions

$$\rho(\theta, \phi)\ ,\ \psi(\theta, \phi) \tag{11}$$

as closely as possible in order to minimize cross-polarized currents in the aperture, for example.

In addition to the parameter ρ_0, we have chosen two other initial parameters for optimization in a three-dimensional space. A second parameter permits *one* degree of freedom in the choice of the initial function ψ_{ϕ_0} (see [1]). For the Cassegrainian design discussed earlier, the value of ψ_{ϕ_0} was selected as unity. The parameter A_ψ is introduced such that

$$\psi_{\phi_0} \equiv 1 + A_\psi \left(\frac{\pi}{180}\right) \sin\phi \tag{12}$$

where A_ψ is given in degrees. The allowable field of A_ψ is bounded to prevent caustics from occurring where not desired. A higher order Fourier series could be used with more parameters available for optimization.

A third parameter used herein was the value of Ω (see Fig. 1 or Fig. 6).

Figure 6 presents the profiles of a three-dimensionally optimized dual-shaped Gregorian reflector pair in the offset plane. A uniform phase in the main reflector aperture was required as indicated by the rays in Fig. 6. The object function was that in Eq. (10). The value θ_0 was chosen as 0.1 deg, while the optimum parameters were found as

$$\rho_0 = 0.015636$$

$$A_\psi = 23.53905^\circ \tag{13}$$

and

$$\Omega = -15.0858^\circ$$

The starting values for the above optimization were chosen from an approximate solution and "manual" optimization through several interations. Table 2 presents an extract of the mapping functions obtained (see Eq. 11).

It is not clear whether this set of "optimum" parameters is global or local. Achieving a rim that is more circular and/or closer to the desired value of $\rho_M = 3$ with better than three significant figures may require greater control of the ψ_{ϕ_0} function (Eq. 12) than one parameter, A_ψ, can provide. Nevertheless, the mapping is approximately circular throughout, i.e.,

$$\rho(\theta, \phi) \approx \rho(\theta) \tag{14}$$

indicating that a low cross-polarization exists in the aperture. Another measure of this low cross-polarization mapping is the *nearly* point caustic illustrated between the Gregorian reflectors in Fig. 6.

Figure 7 illustrates the desired and the achieved aperture power distributions. The desired uniform phase was achieved exactly (see [1]). The small "hole" in the main reflector near $\rho = 0$ is determined by the "optimum" choice of ρ_0. The difference between the geometrical optics (GO) computed power distribution and the desired power near $\rho \approx \rho_M = 3.0$ is at least in part due to the approximate GO analyses used. (The GO analyses utilized a *polar* grid wherein very wide ray "tubes" occur for larger ρ when $\Delta\phi$ is fixed. As $\Delta\phi$ was decreased, it was found that the discrepancy grew smaller for the same set of reflectors.) Similarly, and for the same reason, the small discrepancy near $\rho = 0$ decreased as $\Delta\theta$ was decreased.

A two-dimensional optimization with Ω fixed at $\Omega = -15.0858$ deg, the value found with the three-dimensional optimization, which yields essentially the same reflector pair as illustrated in Fig. 6. In this case, however, the other values chosen for the start of the optimization were $\rho_0 = 0.0001$ and $A_\psi = 0.0$ deg.

Thus, we did not take advantage of the values of ρ_0 and A_ψ known from an approximate solution. The final values of the parameters are shown in Table 3.

It should be noted that in order to achieve the optimized values shown in Table 2 from very poor starting values, a careful construction of constraints had to be built into the optimization algorithm. However, the constraints were general and not limited to any particular geometry.

Table 4 shows the resultant mapping obtained from the two-dimensional algorithm. It is seen that the reflectors obtained in this way differ by very little from those obtained and illustrated in Table 2.

One-dimensional optimizations for an optimum value of ρ_0, with both A_ψ and Ω fixed, are generally less successful unless a reasonably "good" value of A_ψ is chosen. Several cases wherein the starting value of ρ_0 is chosen as:

$$\rho_0(\text{start}) = 0.0001$$

are illustrated in Table 5. Values of

$$A_\psi = 0^\circ$$

$$A_\psi = 10^\circ$$

$$A_\psi = 20^\circ$$

were selected. When either $A_\psi = 0$ deg or $A_\psi = 10$ deg is used, a correct solution is *not* obtained for the PDEs. This is seen by the values of ρ_M obtained at $\theta = 16$ deg. However, when $A_\psi = 20$ deg is chosen, a good solution is obtained. This points up the utility of using the results for ρ_0 and A_ψ from an approximate solution as starting values in any optimization algorithm.

V. Numerical Results for the Gregorian-Type System

The synthesized Gregorian-type low-noise/high-gain dual-shaped offset reflector system was analyzed by GO

during the actual synthesis and with an independent GO computer program. The subreflector was further analyzed by the geometric theory of diffraction (GTD) and by physical optics (PO). The main reflector was analyzed by PO in all cases. Thus, the dual-reflector analysis was performed by GO/PO, GTD/PO, and PO/PO (indicating the subanalysis/main analysis as shown). In addition, the object aperture distribution, Fig. 7, was integrated directly by PO for comparison.

The feed pattern used in the analysis was the same as that used in the synthesis. Principal polarization was chosen as right circular. A projection of the current distribution on the subreflector onto a plane normal to the axis of the feed is shown in Fig. 8. Note the taper of the feed power pattern to -20 dB at the subreflector edge at $\theta = 16$ deg. This sharp taper leads to essentially no spillover loss past the subreflector.

The *equivalent* current aperture distribution on the main reflector is shown in Fig. 9 when the subreflector is analyzed by GO. (The *equivalent* current is the actual current multiplied by the Jacobian determinant transformation of the actual main reflector surface to the aperture plane.) Note that the current distribution is uniform to the point where it then descends Gaussian to approximately -20 dB at the edge of the main reflector. This distribution is essentially the same as the object function in Fig. 7.

The main reflector ($D = 120\lambda$) equivalent current distribution obtained by a GTD subreflector analysis is shown in Fig. 10 (a PO subreflector analysis yields little observable difference). Note the shallow diffraction ripples over most of the aperture (where the current was uniform in Fig. 9). The current distribution still has a Gaussian taper as prescribed in Fig. 7. This will result in very little spillover loss past the main reflector edge and thus be ideal for a low-noise reflector system.

The far-field patterns (diameter of main reflector = 120λ) for each of these analysis cases is shown in Fig. 11. Note the very low loss in gain between the aperture integration of the object function (Fig. 7) and the various diffraction analyses. This illustrates that the chosen object pattern has achieved the goal of potentially very low noise due to spillover past the main reflector into a warm ground environment (typical of upward-looking ground-based antennas). This type of aperture distribution appears achievable only by dual-shaping methods.

VI. Conclusions

When integrating the nonlinear PDEs for offset dual-shaped reflector synthesis from a prescribed outer projected perimeter *inwards*, it was found earlier that computational problems do arise in the central region of the reflectors [1]. It is found herein that these computational problems are largely bypassed if the integration of the PDEs is started from a prescribed projected *inner* rim and integrated *outward*. In this case, however, a circular, or otherwise prescribed, *outer* rim is not guaranteed. In addition, a new parameter of the PDEs is introduced, the radius, ρ_0, of the inner projected rim of the main reflector when the inner value of $\theta = \theta_0$ for the subreflector is prescribed. This parameter exists in addition to other initial parameters (e.g., Ω; see Figs. 1 and 6) and the initial function $\psi_\phi(\phi)$ (see [1]).

A poorly selected inner radius parameter ρ_0, or other poorly selected initial parameters will preclude the obtaining of useful solutions to the PDEs by the method discussed herein or in [1]. Two complementary methods for choosing the parameter ρ_0 and other parameters are discussed. The first method utilizes the initial values found from an approximate solution to the PDEs. A second method utilizes an optimization algorithm which searches for the parameters of the PDEs that minimize a prescribed object function. Such an object function may measure the deviation of the projected outer perimeter from circular (or some other desired shape). Alternatively, a minimum cross-polarization distribution in the aperture (optimum mapping function) may be chosen as the object function.

An offset dual-shaped Cassegrainian-type high-gain antenna is synthesized to illustrate the first method described above. The second method of optimization is illustrated by synthesizing a Gregorian low-noise/high-gain offset dual-shaped reflector antenna. One-parameter [ρ_0], two-parameter [ρ_0 and a parameter A_ψ describing $\psi_{\phi_0}(\phi)$], and three-parameter [ρ_0, A_ψ, and Ω] optimizations are illustrated. Analyses of the synthesized reflectors by GO, GTD, and PO are shown to verify the utility of the results.

It should be noted that the method of using an approximate solution to the PDEs to find the initial parameters is complementary to utilization of the optimization algorithm since it provides an excellent set of starting values for the parameters in the optimization procedure.

Acknowledgments

The authors wish to acknowledge the significant assistance in this work of Prof. S. Rengarajan of California State University at Northridge and R. Hodges, JPL part-time employee and Ph.D. candidate at the University of California at Los Angeles.

References

[1] V. Galindo-Israel, W. Imbriale, and R. Mittra, "On the Theory of Synthesis of Single and Dual Offset Shaped Reflector Antennas," *IEEE Trans. Antennas Propagat.*, vol. AP-35, no. 8, pp. 887–896, August 1987.

[2] J. A. Jervase, R. Mittra, V. Galindo-Israel, and W. Imbriale, "Numerical Study of the Problem of Synthesis of Offset Dual Shaped Reflector Antennas," *URSI/IEEE AP-S Symposium*, pp. 1–2, Syracuse, New York, June 1988.

[3] K. Shogen, V. Galindo-Israel, R. Mittra, and W. Imbriale, "A Numerical Approach for Synthesizing Dual-Shaped Offset Reflector Antennas," presented at URSI/IEEE AP-S Symposium, San Jose, California, June 1989.

Table 1. Comparison of the radiation characteristics of the shaped reflector antenna and the Cassegrainian antenna (see Fig. 5)

Main Reflector	Shaped Reflector	Cassegrainian Antenna
Edge illumination level	−4 dB	−16 dB
−3 dB beamwidth	0.77 deg	0.91 deg
1st sidelobe level	−10 dB	−32 dB

Table 2. Mapping function for three-dimensional optimization, values in Eq. (13)

Values of ρ at:			$\theta°$
$\phi = -90°$ $\psi = +90°$	$\phi = 0°$ $\psi \approx 180°$	$\phi = +90°$ $\psi = 180°$	
0.156359E−01	0.156359E−01	0.156359E−01	0.100000E+00
0.345170E+00	0.353902E+00	0.364169E+00	0.100000E+01
0.691174E+00	0.699794E+00	0.709482E+00	0.200000E+01
0.101939E+01	0.102740E+01	0.103634E+01	0.300000E+01
0.132247E+01	0.132951E+01	0.133745E+01	0.400000E+01
0.159466E+01	0.160053E+01	0.160730E+01	0.500000E+01
0.183220E+01	0.183685E+01	0.184240E+01	0.600000E+01
0.203348E+01	0.203695E+01	0.204135E+01	0.700000E+01
0.219891E+01	0.220133E+01	0.220471E+01	0.800000E+01
0.233064E+01	0.233217E+01	0.233470E+01	0.900000E+01
0.243227E+01	0.243313E+01	0.243500E+01	0.100000E+02
0.251358E+01	0.251401E+01	0.251552E+01	0.110000E+02
0.258565E+01	0.258576E+01	0.258707E+01	0.120000E+02
0.265436E+01	0.265418E+01	0.265537E+01	0.130000E+02
0.272516E+01	0.272466E+01	0.272582E+01	0.140000E+02
0.280943E+01	0.280847E+01	0.280969E+01	0.150000E+02
$\rho_M = 0.301701$E+01	0.301343E+01	0.301529E+01	0.160000E+02

Table 3. Initial value parameters obtained by two-dimensional optimization: starting point: $\rho_0 = 0.0001$, $A_\psi = 0.0°$

Parameters from Two-Dimensional Optimization	
Values Eq. (13)	Values Two-Dimensional Optimization
$\rho_0 = 0.015636$	$\rho_0 = 0.015734$
$A_\psi = 23.53905°$	$A_\psi = 23.30467°$

Table 4. Mapping function for two-dimensional optimization, values in Table 3

Values of ρ at:			
$\phi = -90°$ $\psi = +90°$	$\phi = 0°$ $\psi \approx 0°$	$\phi = +90°$ $\psi = 270°$	$\theta°$
0.157339E−01	0.157339E−01	0.157339E−01	0.100000E+00
0.345189E+00	0.353831E+00	0.364174E+00	0.100000E+01
0.691235E+00	0.699701E+00	0.709547E+00	0.200000E+01
0.101948E+01	0.102728E+01	0.103644E+01	0.300000E+01
0.132259E+01	0.132937E+01	0.133758E+01	0.400000E+01
0.159479E+01	0.160038E+01	0.160745E+01	0.500000E+01
0.183235E+01	0.183667E+01	0.184258E+01	0.600000E+01
0.203364E+01	0.203676E+01	0.204154E+01	0.700000E+01
0.219908E+01	0.220113E+01	0.220491E+01	0.800000E+01
0.233082E+01	0.233197E+01	0.233491E+01	0.900000E+01
0.243246E+01	0.243292E+01	0.243522E+01	0.100000E+02
0.251379E+01	0.251378E+01	0.251576E+01	0.110000E+02
0.258588E+01	0.258550E+01	0.258733E+01	0.120000E+02
0.265463E+01	0.265387E+01	0.265568E+01	0.130000E+02
0.272548E+01	0.272429E+01	0.272618E+01	0.140000E+02
0.280984E+01	0.280797E+01	0.281016E+01	0.150000E+02
ρ_M = 0.301779E+01	0.301343E+01	0.301627E+01	0.160000E+02

Table 5. Parameters and perimeter values from one-dimensional optimization of ρ_0 with A_ψ fixed. Starting point for ρ_0 = 0.0001.

$\phi = -90°$ $\psi = +90°$	$\phi = 0°$ $\psi \approx 180°$	$\phi = +90°$ $\psi = 270°$	$\theta°$
A_ψ = 0.0° Fixed ρ_0 = 0.019594 Final Value			
ρ_0 = 0.195940E−01	0.195940E−01	0.195940E−01	0.100000E+00
ρ_M = 0.542957E+02	0.499525E+02	0.459551E+02	0.160000E+02
A_ψ = 10.0 Fixed ρ_0 = 0.005099 Final Value			
ρ_0 = 0.509900E−02	0.509900E−02	0.509900E−02	0.100000E+00
ρ_M = 0.815349E+00	0.697426E+00	0.299195E+00	0.160000E+02
A_ψ = 20.0 Fixed ρ_0 = 0.01747 Final Value			
ρ_0 = 0.174655E−01	0.174655E−01	0.174655E−01	0.100000E+00
ρ_M = 0.303909E+01	0.300320E+01	0.302680E+01	0.160000E+02

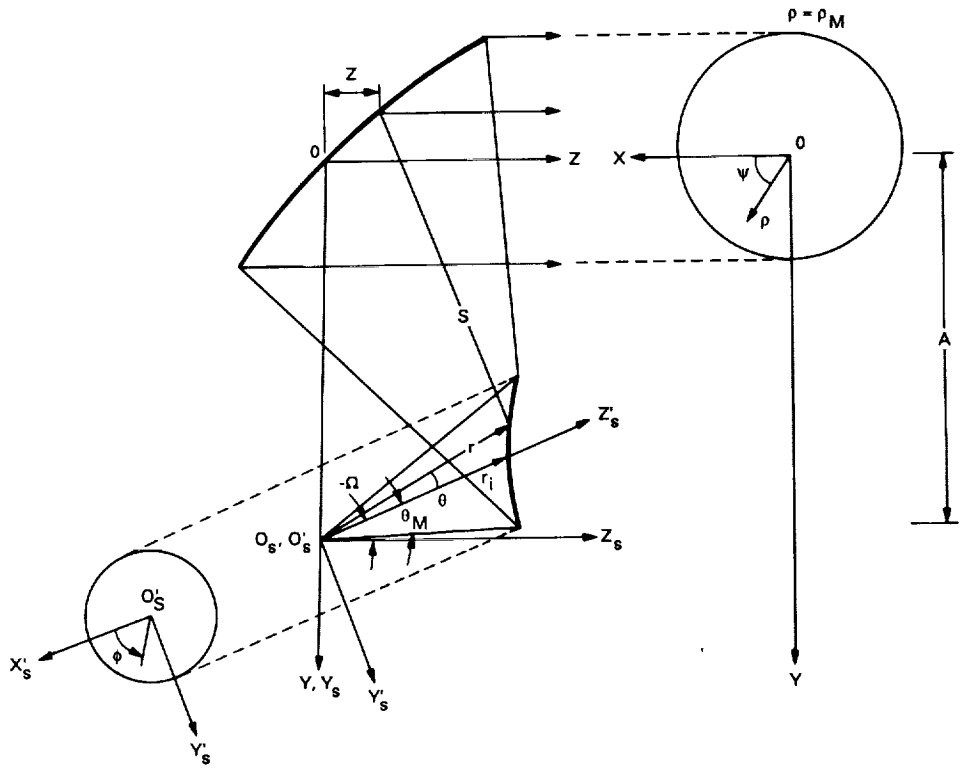

Fig. 1. Geometry of the Cassegrainian-type dual-shaped reflector antenna system.

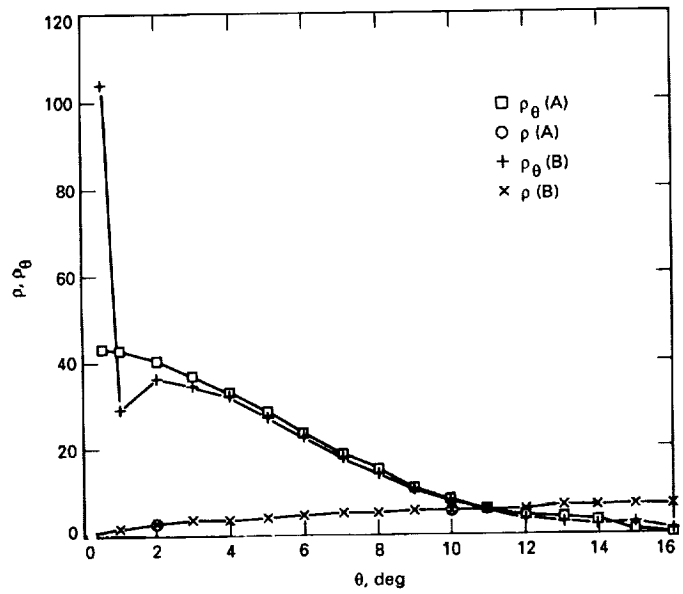

Fig. 2. Variation of ρ and ρ_θ with θ: (a) initial values of ρ_0 obtained from approximate solution and (b) arbitrarily chosen ρ_0.

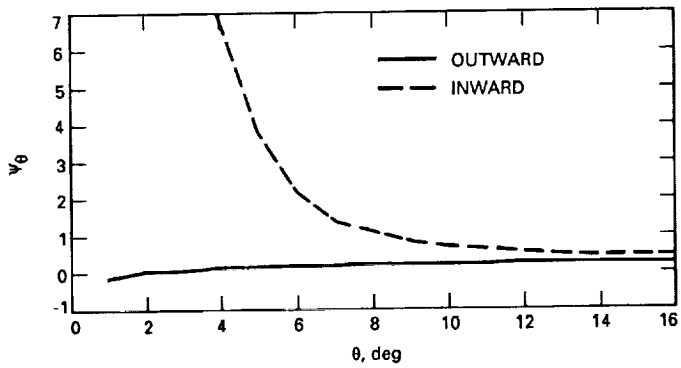

Fig. 3. Variation of $\psi_t\theta$ with θ for an outward and an inward solution.

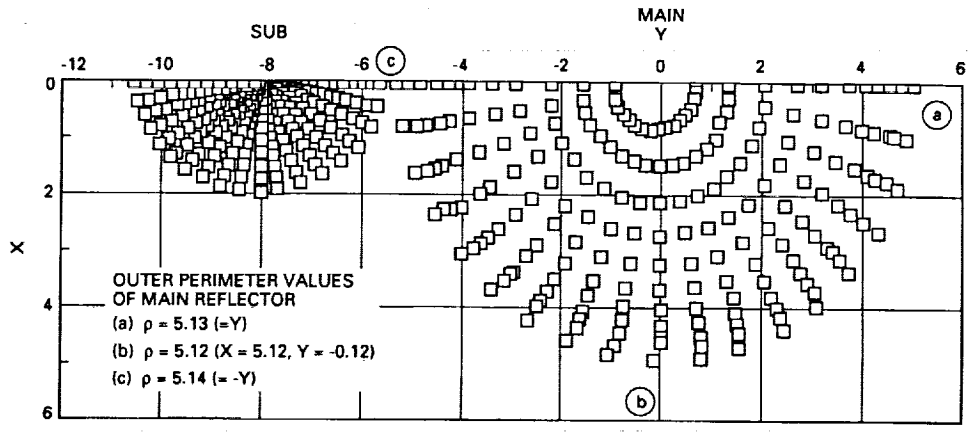

Fig. 4. Cassegrainian-type dual-reflector shape obtained from the synthesis procedure.

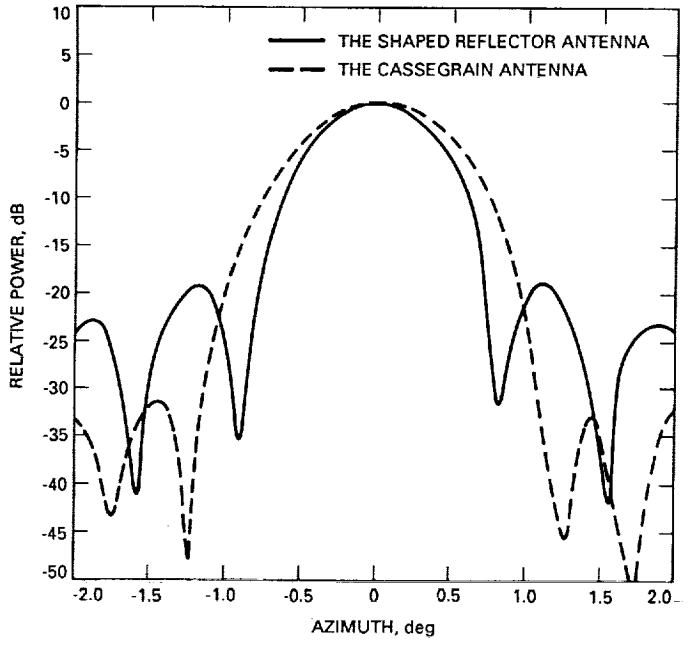

Fig. 5. Comparison of the radiation patterns—Cassegrainian-type case.

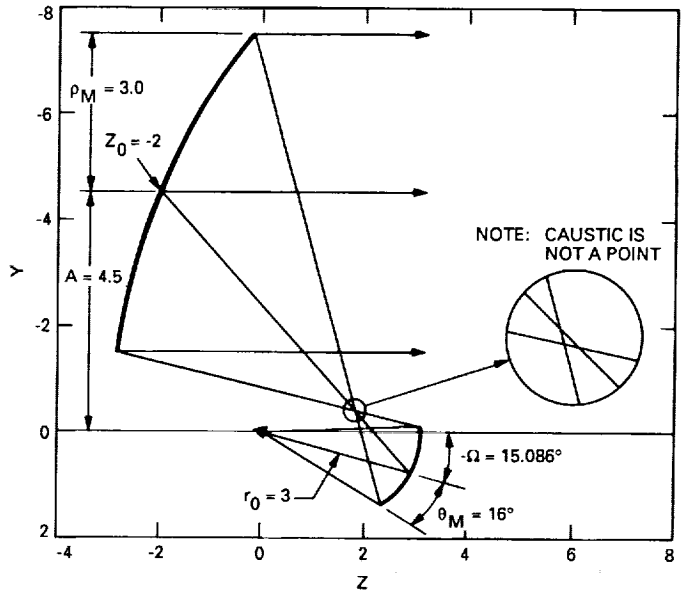

Fig. 6. Dual offset Gregorian reflectors with optimized parameters, ρ_0, A_ψ, and Ω.

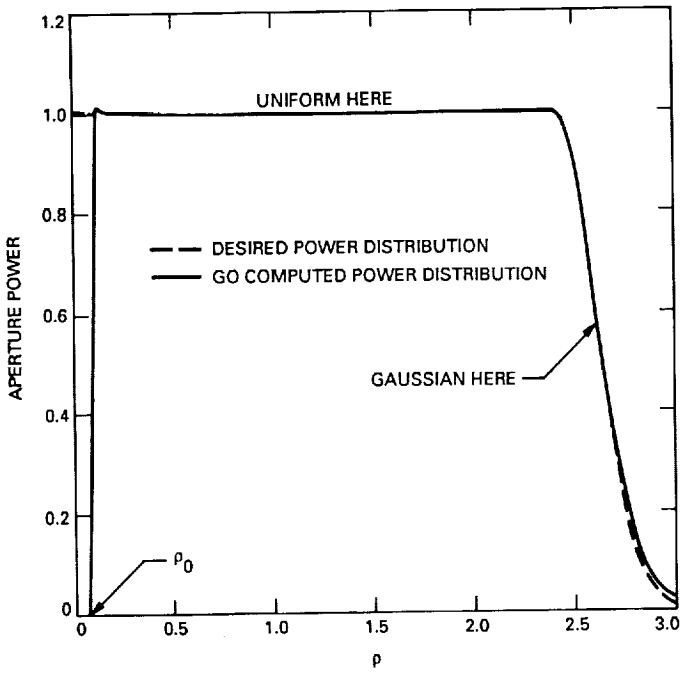

Fig. 7. Main reflector aperture power distributions—desired and computed.

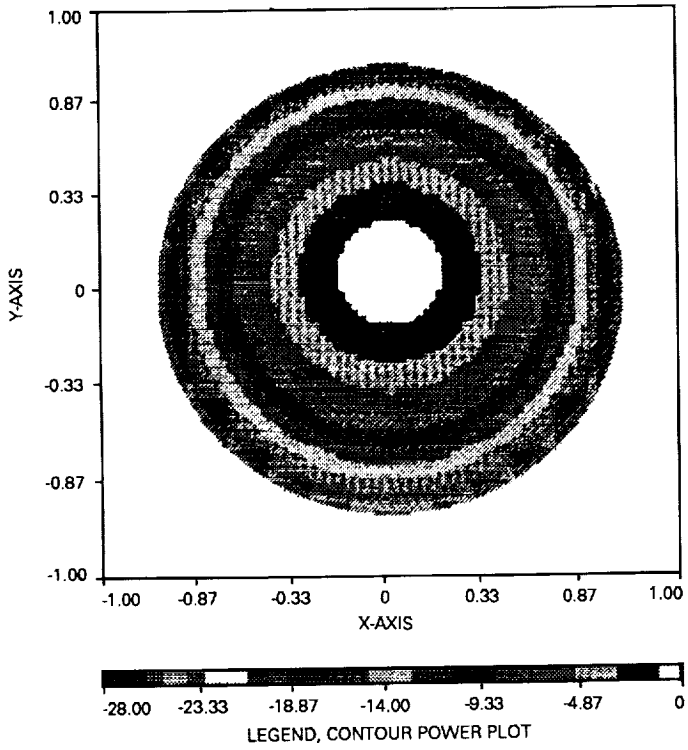

Fig. 8. Feed power pattern—$cos^{116.6}\theta$, projected on $X_s - Y_s$ plane normal to axis of feed.

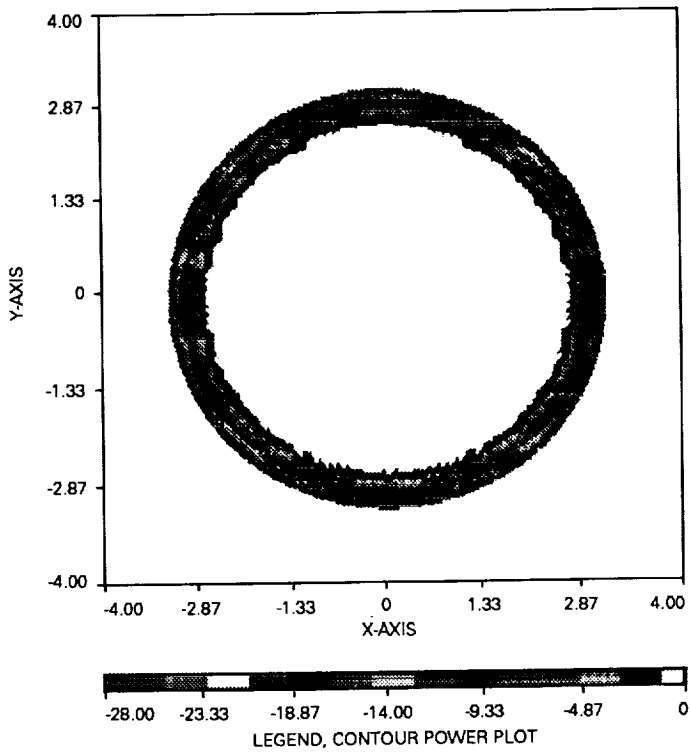

Fig. 9. Equivalent current aperture distribution. Subreflector analysis by GO (see Figs. 7 and 11).

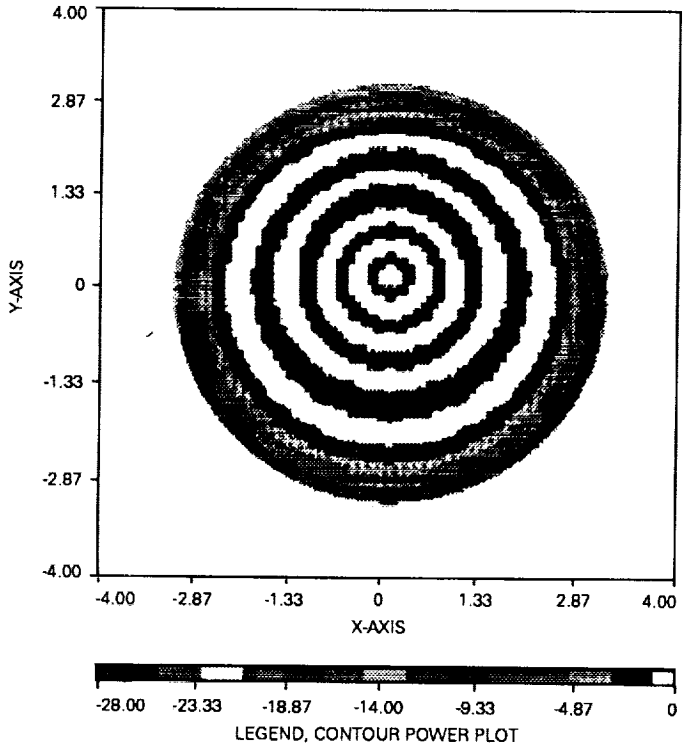

Fig. 10. Equivalent current aperture distribution. Subreflector analysis by GTD (PO analysis yields very similar result, see Fig. 11). Scale: 1 unit = 20λ; radius = 60λ.

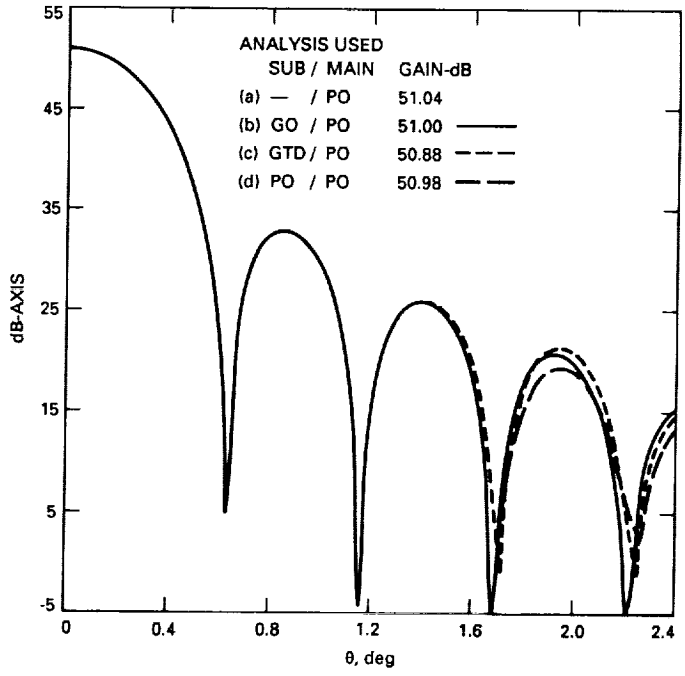

Fig. 11. Gregorian-type dual-reflector far-field power patterns, where $D = 120\lambda$ and feed $E_F = \cos^{58.3}\theta$ (−20 dB at edge of subreflector). Analysis by: (a) aperture PO integration (see Fig. 7); (b) GO for sub and PO for main (see Figs. 7 and 8); (c) GTD/PO (see Fig. 10); and (d) PO/PO (see Fig. 10).